Deep-Space Navigation With Differenced Data Types Part III: An Expanded Information Content and Sensitivity Analysis

J. A. Estefan and S. W. Thurman
Navigation Systems Section

An approximate six-parameter analytic model for Earth-based differenced range measurements is presented and is used to derive a representative analytic approximation for differenced Doppler measurements. The analytical models are tasked to investigate the ability of these data types to estimate spacecraft geocentric angular motion, Deep Space Network station oscillator (clock/frequency) offsets, and signal-path calibration errors over a period of a few days, in the presence of systematic station location and transmission media calibration errors. Quantitative results indicate that a few differenced Doppler plus ranging passes yield angular position estimates with a precision on the order of 0.1 to 0.4 μrad, and angular rate precision on the order of 10 to 25 × 10^{-12} rad/sec, assuming no a priori information on the coordinate parameters. Sensitivity analyses suggest that troposphere zenith delay calibration error is the dominant systematic error source in most of the tracking scenarios investigated; as expected, the differenced Doppler data were found to be much more sensitive to troposphere calibration errors than differenced range. By comparison, results computed using wideband and narrowband ΔVLBI under similar circumstances yielded angular precisions of 0.07 to 0.4 μrad, and angular rate precisions of 0.5 to 1.0 × 10^{-12} rad/sec.

I. Introduction

The analysis described herein represents a follow-up study to two recent work efforts, each separately describing the information content of differenced (two-way minus three-way) range and Doppler radio metric data [1,2]. In these earlier studies, systematic measurement errors induced by observing platform uncertainties, such as baseline coordinate and Earth orientation errors, were not considered. Also excluded from those analyses was an assessment of the effects of transmission media (ionosphere and troposphere) calibration errors on the data. Furthermore, the mathematical models for approximating the differenced range and Doppler measurements were based on the assumption that spacecraft geocentric angular coordinates remained constant over time—a reasonable assump

tion given that the performance characteristics of these data types were investigated for a single tracking pass alone.

In this analysis, the information content of several tracking passes is investigated, with the spacecraft angular coordinates assumed to vary linearly with time. What follows is a detailed derivation of a six-parameter differenced range and Doppler observable model, which is used to assess the performance of these data types under a variety of tracking scenarios. Despite the fact that realistic navigation operations scenarios are not investigated here, due to the relatively short data arc lengths assumed, the selected station (baseline) combinations, and the absence of line-of-sight data such as two-way Doppler or range, the resulting analysis does provide some useful insight into the merit and potential of the differenced data types for navigational purposes. Recall that these "quasi-VLBI" techniques have some operational advantages over the wideband and narrowband ΔVLBI techniques of delta differenced one-way range (ΔDOR) and delta differenced one-way Doppler (ΔDOD) in that the differenced *quasar-less* data can be acquired without interruption of spacecraft command and telemetry activities—a characteristic that may prove invaluable during periods of the approach phase preceding planetary encounters or spacecraft maneuvers. Despite the operational shortcomings of ΔDOR and ΔDOD, it must be acknowledged that they are, for the most part, self-calibrating data types and are therefore less dependent upon accurate externally supplied calibrations of various potential error sources.

II. Observable Models

The mathematical models presented here account for effects due to observing platform and transmission media errors on the differenced data types. As stated previously, several tracking passes are assumed to be acquired, therefore, the angular coordinates are taken to vary over time. Over a period of a few days, the angular motion of an interplanetary spacecraft is nearly linear, hence, the angular rate coordinates of the spacecraft are assumed to be constants for this analysis. Although these assumptions do not significantly affect the formulation of the original differenced range observable arrived at in [1], they do impact the differenced Doppler model; consequently, the observation partial derivatives required for information content and sensitivity analyses become more involved computationally.

A. General Expressions for the Observables

The approximate differenced range observable model is taken to be

$$\Delta\rho \approx \Delta\rho_G + \tau_{tro} + \tau_{ion} + \tau_{clk} \tag{1}$$

where

$\Delta\rho_G$ = differenced range term based purely on geometry

τ_{tro} = delay due to static troposphere calibration errors

τ_{ion} = delay due to static ionosphere calibration errors

τ_{clk} = delay due to station clock and frequency offset and signal-path calibration errors

All delay terms are assumed to be in distance units (i.e., the speed of light factor is dropped for notational convenience). From this formulation, an approximate differenced range-rate observable, proportional to the differenced Doppler observable, follows directly via a time-derivative of Eq. (1), yielding

$$\Delta\dot{\rho} \approx \Delta\dot{\rho}_G + \dot{\tau}_{tro} + \dot{\tau}_{ion} + \dot{\tau}_{clk} \tag{2}$$

in which

$\Delta\dot{\rho}_G$ = differenced Doppler geometric term

$\dot{\tau}_{tro}$ = delay-rate due to the troposphere calibration errors

$\dot{\tau}_{ion}$ = delay-rate due to the ionosphere calibration errors

$\dot{\tau}_{clk}$ = delay-rate due to station and frequency offset calibration errors.

B. Differenced Range and Doppler Geometric Terms

An analytic expression for the differenced range geometric value can be attained by considering the illustrations provided in Figs. 1 and 2. (Fig. 3 illustrates the differenced Doppler and range data acquisition scheme.) From these figures, it is seen that the differenced range geometric term can be expressed as

$$\Delta\rho_G = \mathbf{B} \cdot \left(\frac{\mathbf{r}}{r}\right) = r_B \cos\delta \cos H_B + z_B \sin\delta \tag{3}$$

where

$\mathbf{B}$ = baseline vector between co-observing deep-space stations

$\mathbf{r}$ = spacecraft geocentric position vector

r_B = baseline component normal to the spin axis of Earth

z_B = baseline component parallel to the spin axis of Earth

H_B = baseline hour angle, $\alpha_B - \alpha$

α_B = baseline right ascension, $\alpha_g + \lambda_B$

α_g = Greenwich right ascension

λ_B = baseline longitude

α = spacecraft right ascension

δ = spacecraft declination

The cylindrical baseline coordinates can be expressed as functions of the individual station coordinates, which are defined in Fig. 2, as follows:

$$\left.\begin{aligned} r_B &= \sqrt{(r_{s_1} + r_{s_2})^2 - 2r_{s_1}r_{s_2}[1 + \cos(\lambda_1 - \lambda_2)]} \\ z_B &= z_{h_1} - z_{h_2} \\ \lambda_B &= \tan^{-1}\left(\frac{r_{s_1}\sin\lambda_1 - r_{s_2}\sin\lambda_2}{r_{s_1}\cos\lambda_1 - r_{s_2}\cos\lambda_2}\right) \end{aligned}\right\} \quad (4)$$

where

r_{s_1}, r_{s_2} = station distances from Earth's spin axis

z_{h_1}, z_{h_2} = station distances (height) from Earth's equator

λ_1, λ_2 = station longitudes

Conservative values of station location and baseline coordinate data for three representative DSN stations and their associated baselines are provided in Table 1.[1]

The spacecraft geocentric angular coordinates are approximated by a Taylor series expansion about some reference epoch, t_0

$$\delta = \delta_0 + \dot{\delta}_0(t - t_0) + \cdots$$

$$\alpha = \alpha_0 + \dot{\alpha}_0(t - t_0) + \cdots$$

where

δ_0, α_0 = spacecraft declination and right ascension epoch

$\dot{\delta}_0, \dot{\alpha}_0$ = spacecraft epoch declination rate and epoch right ascension rate

$t - t_0$ = elapsed time from epoch

Higher order terms are not modeled.

A time derivative of Eq. (3) yields the analytic differenced range-rate (Doppler) geometric value

$$\Delta\dot{\rho}_G = -r_B(\dot{H}_B \cos\delta \sin H_B + \dot{\delta}\sin\delta\cos H_B) + z_B\dot{\delta}\cos\delta \quad (5)$$

where

$\dot{H}_B$ = time rate of change of the baseline hour angle

$= \omega - \dot{\alpha}_0$

ω = Earth's rotation rate

$\dot{\delta} = \dot{\delta}_0$

C. Static Troposphere Delay and Delay Rate

Sophisticated empirical models have been developed for tropospheric path delay effects [3].[2] For this study, a much simpler model is used, but one which is still accurate to within about 10 percent of the actual static troposphere path delay for the station–spacecraft elevation angle range of interest ($\geq$10 deg).

A simple troposphere delay model which yields results commensurate with the more complicated empirical models, for elevation angles in excess of about 5 deg, is given by

$$\tau_{tro} = \frac{\tau_{z_{tro}}}{\sin\gamma} \quad (6)$$

where

$\tau_{z_{tro}}$ = zenith troposphere delay

γ = station–spacecraft topocentric elevation angle

[1] T. D. Moyer, "Station Location Sets Referred to the Radio Frame," JPL Interoffice Memorandum 314.5-1334 (internal document), Jet Propulsion Laboratory, Pasadena, California, February 24, 1989.

[2] R. K. Russell, "Computation of Troposphere Partial Derivatives," JPL Technical Memorandum 391-277 (internal document), Jet Propulsion Laboratory, Pasadena, California, February 3, 1972.

In Eq. (6), the zenith delay term, $\tau_{z_{tro}}$, is assumed to represent the *total* zenith troposphere delay. In the empirical models, the delay is typically broken down into separate *wet* and *dry* components.

The model used for differenced range measurements, using Eq. (6), is then given by

$$\tau_{tro} = \left(\frac{\tau_{z_{tro}}}{\sin \gamma}\right)_{sta_1} - \left(\frac{\tau_{z_{tro}}}{\sin \gamma}\right)_{sta_2} \tag{7}$$

The subscripts sta_i, for $i = 1$ and 2, are used to denote each participating tracking station.

A useful modification of Eq. (7) is to express $\sin\gamma$ for each station as a function of spacecraft declination and individual station hour angle, which is accomplished by the following relation:

$$\sin\gamma = \frac{1}{r_{sta}}(r_s \cos\delta \cos H + z_h \sin\delta) \tag{8}$$

where

r_s = station spin radius

z_h = station z-height

H = station hour angle

$r_{sta} = \sqrt{r_s^2 + z_h^2}$

This expression is quite useful when seeking to derive the partial derivatives needed for the sensitivity analyses described later in this article. It should also be noted that each individual station hour angle does not have to be explicitly known as it can be extracted from the baseline hour angle. Let

$$H_2 = H_B - \varphi \tag{9}$$

where

H_2 = hour angle of station 2

φ = baseline longitude relative to station 2

$= \lambda_B - \lambda_2$

Then

$$H_1 = H_2 - (\lambda_2 - \lambda_1) \tag{10}$$

Deriving the troposphere delay-rate model simply requires a time derivative of Eq. (7), thereby yielding

$$\dot{\tau}_{tro} = \left(\frac{\partial \tau_{tro}}{\partial \gamma}\dot{\gamma}\right)_{sta_1} - \left(\frac{\partial \tau_{tro}}{\partial \gamma}\dot{\gamma}\right)_{sta_2} \tag{11a}$$

in which

$$\frac{\partial \tau_{tro}}{\partial \gamma} = \frac{-\tau_{z_{tro}} \cos\gamma}{\sin^2\gamma} \tag{11b}$$

Differentiating Eq. (8) with respect to time, and solving for $\dot{\gamma}$, gives

$$\dot{\gamma} = \frac{1}{r_{sta}\cos\gamma}\left[-r_s\left(\dot{\delta}\sin\delta\cos H + \dot{H}\cos\delta\sin H\right) + z_h\,\dot{\delta}\cos\delta\right] \tag{12}$$

D. Static Ionosphere Delay and Delay Rate

In the previous subsection, it was argued that a very simple, yet accurate, approximation can be used to represent the static troposphere path delay and delay rate. Unfortunately, the behavior of the static ionosphere delay does not lend itself to approximation so easily, as it is dependent upon the location and movement of the Sun with respect to the station–spacecraft line of sight, as well as other elevation-independent parameters [4]. A simple model does exist, however, which approximates the behavior of ionosphere delay as a function of elevation for an "average" homogeneous ionosphere, and it is this model that is utilized for this study.[3]

The ionosphere delay model associated with the differenced range data type is taken to be

$$\tau_{ion} = \left(\frac{A\,\tau_{z_{ion}}}{B + \sin\gamma}\right)_{sta_1} - \left(\frac{A\,\tau_{z_{ion}}}{B + \sin\gamma}\right)_{sta_2} \tag{13}$$

where

$A = 1.15$, $B = 0.15$ } empirical constants that are derived from ray-tracing methods

[3] R. K. Russell, "Computation of Ionosphere Partial Derivatives," JPL Technical Memorandum 391-291 (internal document), Jet Propulsion Laboratory, Pasadena, California, February 29, 1972.

$\tau_{z_{ion}}$ = zenith ionosphere delay

γ = station–spacecraft topocentric elevation angle

The ionosphere delay-rate model for the differenced Doppler is arrived at by differentiating Eq. (13) with respect to time, which gives

$$\dot{\tau}_{ion} = \left(\frac{\partial \tau_{ion}}{\partial \gamma}\dot{\gamma}\right)_{sta_1} - \left(\frac{\partial \tau_{ion}}{\partial \gamma}\dot{\gamma}\right)_{sta_2} \tag{14a}$$

in which

$$\frac{\partial \tau_{ion}}{\partial \gamma} = \frac{-A\ \tau_{z_{ion}} \cos\gamma}{(B + \sin\gamma)^2} \tag{14b}$$

E. Clock Offset and Rate

The station clock offset is modeled as a random ramp, which consists of a random bias term to account for clock offset calibration errors in the ground instrumentation (e.g., hydrogen masers) together with station signal-path calibration errors, and a rate term representing the frequency offset calibration error between the two tracking stations participating in the three-way link.

Mathematically, the clock offset (delay) model can be expressed as

$$\tau_{clk} = \underbrace{b_o + b_{sp}}_{b_T} + f_o(t - t_0) \tag{15}$$

where

b_T = total clock bias, offset (b_o) plus signal-path (b_{sp}), between co-observing stations

f_o = frequency offset between co-observing stations

Second-order effects, such as frequency drift are neglected.

It is easy to derive the clock delay-rate model by virtue of a time-derivative of Eq. (15), which yields

$$\dot{\tau}_{clk} = f_o \tag{16}$$

III. Information Content Analysis

The partial derivatives of any data type represent, to first order, the ability of that data type to sense changes in a spacecraft trajectory. The "information content" of a particular data type is effectively described by the characteristics and behavior of its partial derivatives, and refers to the ability of a data type to determine the various elements that constitute a spacecraft trajectory model. This study specifically explores the information content of differenced range and Doppler for determining geocentric spacecraft angular and angular rate coordinates.

A. Differenced Range and Doppler Partial Derivatives and Error Analysis Formulation

A "linear" model is assumed for the regression equation expressed by

$$\mathbf{z} = A_x \mathbf{x} + \nu \tag{17}$$

where

$\mathbf{z} = [z_1, z_2, \cdots, z_N]^{\mathrm{T}}$, vector of N observations

$\mathbf{x} = \left[\delta_0, \alpha_0, b_{T_1}, b_{T_2}, \cdots, b_{T_{npass}}, \dot{\delta}_0, \dot{\alpha}_0, f_o\right]^{\mathrm{T}}$, vector of parameters to be estimated[4]

$\nu = [\nu_1, \nu_2, \cdots, \nu_N]^{\mathrm{T}}$, vector of N independent Gaussian measurement errors[5]

and A_x is the matrix of vector partial derivatives or partials of the observable, at the time of observation, with respect to the estimated parameter set:

$$A_x = \begin{pmatrix} \partial z_1/\partial \mathbf{x} \\ \partial z_2/\partial \mathbf{x} \\ \cdots \\ \partial z_N/\partial \mathbf{x} \end{pmatrix}$$

In this analysis, the observation set $\mathbf{z}$ contains differenced range and differenced Doppler measurements.

For a weighted least-squares estimator, the statistics associated with the estimation error can be readily computed by using the partial derivative matrix, A_x. A weighted least-squares estimate is one that minimizes the

[4] The subscript *npass* for the clock bias parameter indicates that an independent bias is assumed for each successive tracking pass, since multiple passes are evaluated in this study. An alternative method would be to model the bias as an exponentially correlated process noise parameter with an appropriately selected time constant. The frequency offset is assumed to be stable enough over several passes to warrant only a single representative parameter.

[5] Specifically, the components of ν are assumed to be independent, zero-mean, Gaussian random variables.

weighted sum of squares of the deviations between the actual and predicted (computed) measurements expressed by the scalar, quadratic cost function Q, written as

$$Q = \frac{1}{2}[\mathbf{z} - A_x\hat{\mathbf{x}}]^{\mathrm{T}} W [\mathbf{z} - A_x\hat{\mathbf{x}}] \tag{18}$$

in which $\hat{\mathbf{x}}$ is the "best" estimate of the unknown parameter vector $\mathbf{x}$ (i.e., minimizes the cost function Q) and W is taken to be a symmetric, positive definite weighting matrix. For the special case in which $W = \Gamma_\nu^{-1}$, where Γ_ν is the covariance matrix associated with the data noise vector, ν, the estimate $\hat{\mathbf{x}}$ that minimizes Q is the unbiased, minimum-variance estimate of $\mathbf{x}$, and is given by

$$\hat{\mathbf{x}} = \left(A_x^{\mathrm{T}}\ \Gamma_\nu^{-1} A_x\right)^{-1} A_x^{\mathrm{T}}\ \Gamma_\nu^{-1}\mathbf{z} \tag{19}$$

An important mathematical entity used in performing a statistical error analysis is the information matrix or information array. The information array associated with the estimated parameter set, denoted herein as J_x, can be determined computationally from the matrix of observation partials and the variances associated with each measurement:[6]

$$J_x \equiv A_x^{\mathrm{T}} W A_x = \sum_{i=1}^{N} \frac{1}{\sigma_{\nu_i}^2}\left(\frac{\partial z_i}{\partial \mathbf{x}}\right)^{\mathrm{T}}\left(\frac{\partial z_i}{\partial \mathbf{x}}\right) \tag{20}$$

Equation (20) assumes that the weighting matrix W is diagonal with the ith diagonal element w_i being equal to $1/\sigma_{\nu_i}^2$.

In many of the applications, some initial knowledge is available about a particular parameter or parameters of interest in the form of an unbiased a priori estimate. A priori statistics and the regression equation [Eq. (17)] can be combined to derive a modified form of the weighted least-squares estimator, expressed as

$$\hat{\mathbf{x}} = \left(\tilde{J}_x + A_x^{\mathrm{T}}\ \Gamma_\nu^{-1} A_x\right)^{-1} A_x^{\mathrm{T}}\ \Gamma_\nu^{-1}\mathbf{z} \tag{21}$$

[6] The information array can also be computed analytically using an integral approximation if certain assumptions are made about the sampling rate of the data. This, in fact, was the method employed in the earlier companion studies [1,2]. Unfortunately, for this analysis, the observable models and associated partials are significantly more involved and do not lend themselves to easy analytical derivation of the information arrays.

The term $\tilde{J}_x$ denotes the a priori information array and is usually taken to be equal to the inverse of $\tilde{\Gamma}_x$, the initial covariance matrix for $\mathbf{x}$.[7]

From this development, the estimated or computed error covariance matrix, denoted $\Gamma_{x_{comp}}$, can readily be determined

$$\Gamma_{x_{comp}} \equiv E\left[(\mathbf{x} - \hat{\mathbf{x}})(\mathbf{x} - \hat{\mathbf{x}})^{\mathrm{T}}\right] = \left(\tilde{J}_x + J_x\right)^{-1} \tag{22}$$

For differenced range measurements, the observation partials are found to be

$$\begin{aligned}\left(\frac{\partial \Delta\rho}{\partial \mathbf{x}}\right)^{\mathrm{T}} &= \frac{\partial \Delta\rho}{\partial\left[\delta_0, \alpha_0, b_{T_1}, b_{T_2}, \ldots, b_{T_{npass}}, \dot{\delta}_0, \dot{\alpha}_0, f_o\right]} \\ &= [-r_B \sin\delta\cos H_B + z_B\cos\delta, \\ &\quad r_B\cos\delta\sin H_B, 1, 1, \ldots, 1_{npass}, \\ &\quad (\partial\Delta\rho/\partial\delta_0)(t - t_0),\ (\partial\Delta\rho/\partial\alpha_0)(t - t_0), \\ &\quad t - t_0]\end{aligned} \tag{23}$$

and follow directly from the observable models provided in Section II.

For the case of differenced Doppler measurements, by letting $\dot{H}_B \rightarrow \omega$ (since $\dot{\alpha}_0 \ll \omega$) and substituting $\dot{\delta} = \dot{\delta}_0$, the observation partials are found to be

$$\begin{aligned}\left(\frac{\partial \Delta\dot{\rho}}{\partial \mathbf{x}}\right)^{\mathrm{T}} &= \frac{\partial \Delta\dot{\rho}}{\partial\left[\delta_0, \alpha_0, b_{T_1}, b_{T_2}, \ldots, b_{T_{npass}}, \dot{\delta}_0, \dot{\alpha}_0, f_o\right]} \\ &= \left[r_B\left(\omega\sin\delta\sin H_B - \dot{\delta}_0\cos\delta\cos H_B\right) - z_B\dot{\delta}_0\sin\delta,\right. \\ &\quad r_B\left(\omega\cos\delta\cos H_B - \dot{\delta}_0\sin\delta\sin H_B\right), 0, 0, \ldots 0_{npass}, \\ &\quad (-r_B\sin\delta\cos H_B + z_B\cos\delta) + (\partial\Delta\dot{\rho}/\partial\delta_0)(t - t_0), \\ &\quad \left. r_B\cos\delta\sin H_B + (\partial\Delta\dot{\rho}/\partial\alpha_0)(t - t_0),\ 1\right]\end{aligned} \tag{24}$$

[7] Generally speaking, the a priori information array need not be invertible. Furthermore, Eq. (21) represents a "normalized" form of the weighted least-squares estimator in which estimates are made of the corrections to the a priori values, hence, the a priori estimate of the parameter vector $\mathbf{x}$ is assumed to be zero.

B. Error Covariance Calculations (Part 1)

Recall that the baseline hour angle varies linearly with time and can be expressed as

$$H_B = H_{B_0} + \omega (t - t_0) \tag{25}$$

where

H_{B_0} = epoch baseline hour angle

$\omega t_0 = \alpha_0$

For this study, a "symmetric" tracking pass was assumed about H_{B_0} from which lower and upper limits on the baseline hour angle were used to accumulate the differenced range and Doppler information array given in Eq. (20). The lower and upper baseline hour angle limits, H_{B_l} and H_{B_u}, respectively, were taken to be

$$H_{B_l}, H_{B_u} = H_{B_0} - \Psi, H_{B_0} + \Psi \tag{26}$$

where

$\Psi \equiv$ tracking pass half-width.

A suitable choice for the tracking pass width 2Ψ was made for each candidate baseline by constraining the minimum elevation angle at each participating station to be approximately 10 deg. A more detailed description of this geometric dependence and suitable choices of 2Ψ for the DSN Canberra–Goldstone and Madrid–Goldstone baselines are provided in [1]. For the Canberra–Goldstone baseline, it was found that a constant tracking pass half-width value of 30 deg (about four hours' worth of continuous tracking) could be obtained for the range of spacecraft declination angles studied: -20 deg $\leq \delta \leq 20$ deg. In terms of data noise characteristics, the data accuracy for the differenced Doppler and range measurements were taken to be somewhat conservative by the standards of earlier analyses; specifically, measurement uncertainties were taken to be $\sigma_{\Delta\dot{\rho}} = 0.15$ mm/sec and $\sigma_{\Delta\rho} = 30.0$ cm. A 60-sec sampling rate was used for differenced Doppler and one differenced range point was acquired every 300 sec.

No a priori statistics were assumed for the spacecraft angular coordinate parameters to be estimated by the filter $(\delta_0, \alpha_0, \dot{\delta}_0, \dot{\alpha}_0)$. Conversely, a priori information was assumed to be available for the clock bias (offset/signal path) and frequency offset parameters, based on extrapolations of current DSN ranging and calibration system capabilities. The a priori information array $\tilde{J}_x$ was thus taken to be

$$\tilde{J}_x = \text{diag}\left[0, 0, \left(\frac{1}{\sigma_{b_{T_1}}}\right)^2, \left(\frac{1}{\sigma_{b_{T_2}}}\right)^2, \cdots, \left(\frac{1}{\sigma_{b_{T_{npass}}}}\right)^2, 0, 0, \left(\frac{1}{\sigma_{f_o}}\right)^2\right] \tag{27}$$

where

$\sigma_{b_{T_i}}$ = one-sigma a priori clock offset/signal-path uncertainty for the ith tracking pass

σ_{f_o} = one-sigma a priori frequency offset uncertainty

One-sigma uncertainties for the clock offset/signal-path and frequency offset parameters were assumed to be $\sigma_{b_{T_i}} =$ 10 nsec (~300 cm) and $\sigma_{f_o} = 0.02$ mm/sec, respectively.

Preliminary error analysis results for differenced range tracking from the DSN Canberra–Goldstone baseline suggest that the data are capable of determining spacecraft angular position coordinates to a precision of about 0.04 to 0.3 μrad (computed-only results) at the conclusion of five successive tracking passes, over the range of declinations investigated. The geocentric angular rate terms are seen to be determined within a range of 10 to 20 $\times 10^{-12}$ rad/sec. These results illustrate the difficulty which differenced range data have in being able to accurately sense spacecraft angular motion in the absence of other data types and a priori information. Differenced Doppler measurements were consequently used to augment the differenced range with computed-only results, which suggested that the two data types, when used in concert, can yield precisions on the order of 0.02 to 0.2 μrad for the geocentric angular coordinates and a reduction in the angular rate uncertainty to 3 to 8 $\times 10^{-12}$ rad/sec, again, at the conclusion of five successive tracking passes. The full set of these results is summarized in Table 2, which provides the one-sigma uncertainties for estimated parameters over the course of five tracking passes.

It is interesting that the best performance is seen at the smaller declination magnitudes. Although this is contrary

to the behavior seen in earlier studies [1,2], one must remember that the spacecraft angular coordinates were assumed to remain "fixed" over the evolution of tracking passes considered, whereas in this study, the data must also attempt to determine the angular rate terms. Without adequate initial knowledge of these parameters, the filter, hence the data, must work extremely hard not only to determine the spacecraft angular coordinates and rates, but the clock/clock-rate offsets as well.

It is well known that unmodeled delays due to clock offset and station signal path calibration errors can be a major factor preventing differenced range data from yielding angular precisions comparable to those of ΔVLBI data, and the addition of differenced Doppler data will not necessarily help, as they are nearly insensitive to clock offsets. For this reason, another error covariance calculation was made with a "tighter" a priori knowledge of the clock biases, assuming an advanced DSN ground calibration system emplaced, e.g., a DSN Global Positioning System (GPS) Ground Calibration System.[8] For these cases, the one-sigma a priori uncertainty in the clock offset was assumed to be 1 nsec (~30 cm). Because the epoch declination estimate is most affected by the uncertainty in the station clock offset, only the improvement in declination precision is shown (see Fig. 4). The results shown in Fig. 4 indicate that the ability of the differenced range data to determine the clock bias parameters is relatively weak in the near-zero declination regime; this is reflected in the more dramatic improvement seen for the tighter clock synchronization value, as is evident in the same figure, and the lesser improvement seen for the higher declination magnitudes. The inability of the filter to reduce the uncertainty in frequency offset is a reflection of its current highly precise calibration value.

A similar assessment was made for a DSN Madrid–Goldstone baseline, however, there are some important differences in terms of viewing constraints and tracking geometries that need to be noted before summarizing the error analysis results. The fact that both DSN complexes (Madrid and Goldstone) are located in the Northern Hemisphere severely restricts the tracking-pass width, and hence, the amount of available data at low declinations ($\delta \leq 5$ deg). The result, as seen in the earlier companion studies, is a severe degradation in precision at these lower declination angles. Furthermore, there is an inherent difficulty in being able to determine the spacecraft declination in the near-zero region resulting from the relatively small magnitude of the baseline z-height component, as compared with the Canberra–Goldstone baseline (see Table 1). The available overlap increases dramatically for the higher declination magnitudes ($\delta \leq 10$ deg). For this analysis, a tracking-pass half-width value of 30 deg was selected for $\delta = 10$ deg, and a value of 37 deg was chosen for the $\delta = 20$-deg case, which translates to about four and five hours of continuous tracking, respectively. (Note that the lower declination magnitude cases are ignored for this baseline for reasons just cited.)

Estimation statistics for the Goldstone–Madrid baseline are summarized in Table 3, in which identical assumptions on data-sampling rate and measurement accuracy characteristics are made as for the Canberra–Goldstone study, as well as on the a priori statistics. Results suggest that the differenced data types can together deliver about 0.2- to 0.5-μrad precision for the geocentric angular coordinates and about 3×10^{-12} to 40×10^{-12}-rad/sec precision for the angular rates, at the conclusion of five successive tracking passes. Clearly, the Canberra–Goldstone baseline results are superior for the $\delta = 10$-deg case by about a factor of three in which the same tracking-pass half-width value was assumed ($\Psi = 30$ deg). For the 20-deg case, on the other hand, better performance is seen for the Madrid–Goldstone baseline in terms of being able to determine the epoch declination and measurement biases. This should not be surprising, however, as a larger tracking-pass half-width value was employed ($\Psi = 37$ deg) than with the Canberra–Goldstone case. In fact, even with the increase in data volume, the determination of the epoch right ascension parameter and angular rate terms was poorer than with the Canberra–Goldstone baseline. Although the Madrid–Goldstone baseline offers a greater availability of data over the Canberra–Goldstone baseline, as the spacecraft declination angle increases, the latter offers the more favorable results in terms of angular precision.

IV. Sensitivity Analysis

A useful analysis tool is the sensitivity matrix method, which is frequently used in orbit determination error analyses and provides a means to distinguish among the effects of several different unmodeled systematic error sources on the parameter estimates [5,6]. Knowledge of the sensitivity matrix enables one to compute the full-consider error covariance matrix, which accounts for the computed uncertainty due purely to random measurement noise *plus* the uncertainty induced by unmodeled consider parameters.[9]

[8] S. M. Litchen, "GPS-Based DSN Calibration System (RTOP 61)," (presentation viewgraphs), Office of Spaceflight Operations Advanced Systems Review, DSN Advanced Systems Program, Jet Propulsion Laboratory, Pasadena, California, June 18–19, 1991.

[9] Recall that a consider parameter is treated by the filter as an unmodeled systematic error source.

A. Filter Augmentation

The original regression equation, Eq. (17), is augmented with an additional term, which results in a regression equation of the form

$$\mathbf{z} = A_x\mathbf{x} + A_y\mathbf{y} + \nu \tag{28}$$

where

$\mathbf{z} = [z_1, z_2, \cdots, z_N]^{\mathrm{T}}$, vector of N observations

$\mathbf{x} = \left[\delta_0, \alpha_0, b_{T_1}, b_{T_2}, \cdots, b_{T_{npass}}, \dot{\delta}_0, \dot{\alpha}_0, f_o\right]^{\mathrm{T}}$, vector of original estimated parameters

$\mathbf{y} = \left[r_B, z_B, \lambda_B, \tau_{z_{tro_1}}, \tau_{z_{tro_2}}, \tau_{z_{ion_1}}, \tau_{z_{ion_2}}\right]^{\mathrm{T}}$, vector of considered parameters

$\nu = [\nu_1, \nu_2, \cdots, \nu_N]^{\mathrm{T}}$, vector of N independent Gaussian measurement errors

and A_x is, again, the matrix of observation partials with respect to the estimated parameter set, while A_y is the matrix of observation partials with respect to the considered parameter set:

$$A_x = \begin{pmatrix} \partial z_1/\partial \mathbf{x} \\ \partial z_2/\partial \mathbf{x} \\ \cdots \\ \partial z_N/\partial \mathbf{x} \end{pmatrix}, \qquad A_y = \begin{pmatrix} \partial z_1/\partial \mathbf{y} \\ \partial z_2/\partial \mathbf{y} \\ \cdots \\ \partial z_N/\partial \mathbf{y} \end{pmatrix}$$

The sensitivity matrix, denoted S_{xy}, is defined to be

$$S_{xy} \equiv \frac{\partial \hat{\mathbf{x}}}{\partial \mathbf{y}} = \frac{\partial \hat{\mathbf{x}}}{\partial \mathbf{z}}\left(\frac{\partial \mathbf{z}}{\partial \mathbf{y}}\right)$$

$$= \Gamma_{x_{comp}} J_{xy} \tag{29}$$

where

$$J_{xy} \equiv A_x^{\mathrm{T}} W A_y = \sum_{i=1}^{N} \frac{1}{\sigma_{\nu_i}^2}\left(\frac{\partial z_i}{\partial \mathbf{x}}\right)^{\mathrm{T}}\left(\frac{\partial z_i}{\partial \mathbf{y}}\right) \tag{30}$$

Once again, it is assumed in Eq. (30), that the weighting matrix W, is diagonal.

For differenced range measurements, based on the observable development given in Section II and a substitution of the empirical ray-tracing constants for the static ionosphere delay model, the consider observation partials are found to be

$$\left(\frac{\partial \Delta\rho}{\partial \mathbf{y}}\right) = \frac{\partial \Delta\rho}{\partial\left[r_B, z_B, \lambda_B, \tau_{z_{tro_1}}, \tau_{z_{tro_2}}, \tau_{z_{ion_1}}, \tau_{z_{ion_2}}\right]^{\mathrm{T}}}$$

$$= \Big[\cos\delta\cos H_B,\ \sin\delta,\ -\partial\Delta\rho/\partial\alpha_0,$$

$$r_{sta_1}/(r_{s_1}\cos\delta\cos H_1 + z_{h_1}\sin\delta),$$

$$-r_{sta_2}/(r_{s_2}\cos\delta\cos H_2 + z_{h_2}\sin\delta),$$

$$1.15r_{sta_1}/(0.15r_{sta_1} + r_{s_1}\cos\delta\cos H_1 + z_{h_1}\sin\delta),$$

$$-1.15r_{sta_2}/(0.15r_{sta_2} + r_{s_2}\cos\delta\cos H_2 + z_{h_2}\sin\delta)\Big]^{\mathrm{T}} \tag{31}$$

In the case of differenced Doppler measurements, the consider observation partials are found, upon further substitution of $\dot{H}_B = \omega$ and $\dot{\delta} = \dot{\delta}_0$, to be

$$\left(\frac{\partial \Delta\dot{\rho}}{\partial \mathbf{y}}\right) = \frac{\partial \Delta\dot{\rho}}{\partial \left[r_B, z_B, \lambda_B, \tau_{z_{tro_1}}, \tau_{z_{tro_2}}, \tau_{z_{ion_1}}, \tau_{z_{ion_2}}\right]^{\mathrm{T}}}$$

$$= \Bigg[-\omega \cos\delta \sin H_B - \dot{\delta}_0 \sin\delta \cos H_B,\ \dot{\delta}_0 \cos\delta,\ -\partial\Delta\dot{\rho}/\partial\alpha_0,$$

$$\frac{1}{r_{sta_1} \sin^2 \gamma_{s_1}} \left[r_{s_1}\left(\dot{\delta}_0 \sin\delta \cos H_1 + \omega \cos\delta \sin H_1\right) - z_{h_1}\dot{\delta}_0 \cos\delta\right],$$

$$\frac{1}{r_{sta_2} \sin^2 \gamma_{s_2}} \left[-r_{s_2}\left(\dot{\delta}_0 \sin\delta \cos H_2 + \omega \cos\delta \sin H_2\right) + z_{h_2}\dot{\delta}_0 \cos\delta\right],$$

$$\frac{1.15}{r_{sta_1}(0.15 + \sin\gamma_{s_1})^2} \left[r_{s_1}\left(\dot{\delta}_0 \sin\delta \cos H_1 + \omega \cos\delta \sin H_1 + \omega\cos\delta\sin H_1\right) - z_{h_1}\dot{\delta}_0 \cos\delta\right],$$

$$\frac{1.15}{r_{sta_2}(0.15 + \sin\gamma_{s_2})^2} \left[-r_{s_2}\left(\dot{\delta}_0 \sin\delta \cos H_2 + \omega \cos\delta \sin H_2\right) + z_{h_2}\dot{\delta}_0 \cos\delta\right]\Bigg]^{\mathrm{T}} \tag{32}$$

The computation of the total or full-consider error covariance matrix, denoted $\Gamma_{x_{cons}}$, is given by

$$\Gamma_{x_{cons}} = \Gamma_{x_{comp}} + S_{xy}\ \Gamma_y\ S_{xy}^{\mathrm{T}} \tag{33}$$

where

$\Gamma_{x_{comp}}$ = computed error covariance matrix

S_{xy} = sensitivity matrix

Γ_y = consider parameter covariance matrix

The considered parameters are assumed to be uncorrelated, thus Γ_y is diagonal, with the associated consider variances as principal diagonal entries:

$$\Gamma_y = \mathrm{diag}\left[\sigma_{r_B}^2, \sigma_{z_B}^2, \sigma_{\lambda_B}^2, \sigma_{\tau_{z_{tro_1}}}^2, \sigma_{\tau_{z_{tro_2}}}^2, \sigma_{\tau_{z_{ion_1}}}^2, \sigma_{\tau_{z_{ion_2}}}^2\right] \tag{34}$$

This leads to the introduction of the perturbation matrix, denoted P_{xy}, and defined as

$$P_{xy} \equiv S_{xy}\sqrt{\Gamma_y} = S_{xy}\ \mathrm{diag}\left[\sigma_{r_B}, \sigma_{z_B}, \sigma_{\lambda_B}, \sigma_{\tau_{z_{tro_1}}}, \sigma_{\tau_{z_{tro_2}}}, \sigma_{\tau_{z_{ion_1}}}, \sigma_{\tau_{z_{ion_2}}}\right] \tag{35}$$

The perturbation matrix is another useful analysis tool as it indicates the one-sigma perturbation of each estimated parameter due to each consider parameter [6]. This information can be used to evaluate the impact of each individual consider parameter on the estimated parameter uncertainties or used to lump the effects into various groups of error sources; in this case, into observing platform errors and transmission media delay calibration errors.

The one-sigma uncertainties for the considered parameters are taken to be

$$\left.\begin{aligned} \sigma_{r_B} &= 12.6\ \mathrm{cm} \\ \sigma_{z_B} &= 13.0\ \mathrm{cm} \\ \sigma_{\lambda_B} &= 39.8\ \mathrm{nrad} \end{aligned}\right\} \text{(observing platform)}$$

$$\left.\begin{aligned} \sigma_{\tau_{tro_{1,2}}} &= 4.0\mathrm{cm} \\ \sigma_{\tau_{ion_{1,2}}} &= 5.0\mathrm{cm} \end{aligned}\right\} \text{(transmission media)}$$

These baseline coordinate uncertainties are representative of the combined uncertainty due to current levels of relative station location error and Earth orientation calibration error [7]. The troposphere zenith delay values are consistent with current DSN calibration capabilities, and the ionosphere zenith delay values reflect that X-band (8.4-GHz) radio link frequencies are assumed.

B. Error Covariance Calculations (Part 2)

Several cases were run to determine the effects of unmodeled systematic errors on the differenced Doppler and range data. In Tables 4 and 5, error statistics for the reference DSN Canberra–Goldstone and Madrid–Goldstone baseline cases using differenced Doppler together with differenced range over the evolution of five successive tracking passes are shown. These results reflect the *total* error in which the uncertainty due to the consider parameters is combined with the estimated parameter uncertainty due to measurement noise to better reflect "real world" results. Here, it is seen that the consider parameter effects can be quite substantial, even after several passes of data have been acquired. Although the estimated clock delay terms are only marginally affected by the unmodeled error sources, the parameters constituting the spacecraft angular motion are more severely impacted.

For the Canberra–Goldstone baseline, the most affected parameter is seen to be the epoch right ascension in which up to a seven-fold degradation in performance is evident at zero declination (see Tables 2 and 4) and about a four-fold degradation at the lowest and highest declination magnitudes (recall that symmetric passes are assumed). Degradation was less severe for the estimated epoch declination parameter yet still significant; about an 85-percent degradation at the extreme declination magnitudes and about a 23-percent degradation in the zero declination region. The angular rate parameters are degraded by about a factor of two to three-and-a-half times the nominal (computed) values over the selected declination range. In the case of the Madrid–Goldstone baseline, the error statistics suggest that the most heavily impacted parameter is epoch declination, especially for the 10-deg declination case; the resulting performance is shown to be quite poor, even after five successive tracking passes. In the 20-deg declination case, an approximate three-fold degradation in epoch declination determination is seen over the computed-only results, and the determination of epoch right ascension is degraded by about one-and-a-half times the estimated result. To gain insight into whether the observed degradation was due primarily to baseline coordinate errors or transmission media delay calibration errors, the one-sigma perturbations due to each consider parameter were computed (i.e., the perturbation matrix). The perturbations due to "lumped" error sources are shown in Fig. 5 for the Canberra–Goldstone baseline case. Clearly, the troposphere is the dominant error source in almost all cases. Generally speaking, the effects of baseline coordinate uncertainties are not seen to be significant.

As a result of these findings, a focus on reducing the effects of tropospheric path delay errors was made[10] that was attempted in two ways: (1) using a more accurate zenith delay calibration and (2) raising the elevation cutoff angles at the two stations constituting the baseline. Another possible strategy, which would require further research, would be the use of an elevation-dependent data-weighting function, such as the one that was recently developed for two-way X-band (8.4-GHz) Doppler [8,9]. The results obtained with these techniques are illustrated in Fig. 6, for the most severely affected estimated parameter—epoch right ascension. Here, it is seen that the most dramatic improvement results from a smaller zenith delay calibration error value, taken to be 2 cm in this case, which could be achieved by an improved DSN ground calibration system. The more interesting curve results from the higher elevation cutoff (approximately 15 deg) in which the reduction in uncertainty is also seen to be substantial. These results indicate that an elevation cutoff of 15 deg (or perhaps higher) could yield significantly improved performance over the results given in Tables 4 and 5 for a 10-deg cutoff, even without the benefit of an improved troposphere calibration technique.

V. Remarks

Differenced Doppler and range measurements acquired from multiple baselines were not addressed in this analysis. Results from the earlier companion studies suggested that if knowledge of DSN station clock offsets was assumed to be relatively large, angular precision for cases involving longer differenced data arcs from a single baseline were superior to the shorter data arcs acquired from two different baselines [1,2]. This, of course, was a reflection of a greater amount of data available to the filter for estimating clock offsets. For studies involving more optimistic assumptions about the DSN's ability to calibrate station clock offsets, better performance was observed for the dual baseline cases over the single baseline cases, despite the shorter data arcs used from each of the two individual baselines. Another tracking strategy that has been

[10] For the Canberra–Goldstone baseline case only.

suggested is to alternate data acquisition from the DSN baselines on a per-pass basis in an effort to further reduce the sensitivity of the differenced data types to transmission media delay effects; this, however, will require further study.[11]

To provide a reference point for comparison with the differenced range and Doppler results, angular precision and angular rate precision estimates were computed for both wideband ΔVLBI (ΔDOR) and narrowband ΔVLBI (ΔDOD) data acquired from a single baseline over a period of a few days. In these calculations, it was assumed that one ΔDOR measurement and one ΔDOD measurement were acquired simultaneously each day from the DSN Goldstone–Canberra baseline for five successive days. The measurement accuracies assumed for these data were 20 cm for ΔDOR, and 0.05 mm/sec for ΔDOD; these measurement accuracies are representative of the performance that can be achieved at X-band (8.4-GHz) frequencies.[12] The results for five different declination values ranging from −20 deg to +20 deg are given in Table 6. The baseline hour angle for each pair of ΔDOR/ΔDOD measurements was chosen so that a spacecraft at the specified declination angle would be observed at or near the maximum elevation angle from both the Goldstone and Canberra complexes. Small departures of up to 10 deg in the baseline hour angle away from this configuration were intentionally made so as to vary the observing geometry some, although no attempt was made to choose the baseline hour angles for each day in such a way as to optimize the results.

Compared with the differenced range and Doppler results given in Tables 4 and 5, the data in Table 6 show comparable angular precision (about 0.07 to 0.04 μrad), but much better angular rate precision than the differenced range and Doppler data (0.5×10^{-12} to 1.0×10^{-12} rad/sec as opposed to 7×10^{-12} to 25×10^{-12} rad/sec). A comparison of Table 6 with the ideal (no systematic error source effects) differenced range/Doppler precision data given in Tables 1 and 2 indicates that the ideal angular precision obtained with differenced range/Doppler data is much closer to that obtained with ΔVLBI data, but that the ΔVLBI data still yield the greatest angular precision even in this scenario.

VI. Conclusions

The simple three-parameter analytic differenced range and Doppler observable models that were developed in the previous studies were refined in this analysis into more-detailed six-parameter observable models in order to ascertain the ability of these data types to estimate both spacecraft angular coordinates and DSN clock/frequency offsets, as well as spacecraft angular rate coordinates, over a tracking period of a few days. Furthermore, the expanded models incorporated systematic station location and transmission media (troposphere/ionosphere) calibration errors which were not addressed previously.

Error covariance calculations suggested that a few differenced Doppler plus ranging passes were capable of yielding angular position estimates with a precision on the order of 0.1 to 0.4 μrad, and an angular rate precision on the order of 3 to 25×10^{-12} rad/sec—this in the absence of any a priori statistical information on the coordinate parameters. Results based on sensitivity analysis calculations suggested that the most dominant systematic error source in most of the tracking scenarios that were investigated was troposphere zenith delay calibration error. As expected, the differenced Doppler data were found to be more sensitive to troposphere calibration errors than the differenced range data. However, it was also discovered that by raising the elevation cutoff to 15 deg at both stations constituting the baseline, the effects due to troposphere calibration errors were significantly reduced. A similar, yet even more dramatic improvement was seen when an improved zenith delay value was chosen based on an advanced DSN ground calibration system employing GPS measurements. These quantitative results were based strictly on the differenced data types themselves, as no additional radio metric data types were assumed, e.g., two-way (coherent) Doppler and/or range. It must be remembered that in an operational environment, the differenced data types would be used in conjunction with conventional line-of-sight tracking data types (two-way range/Doppler), however, further study is needed to establish navigation accuracy estimates for more realistic scenarios. For comparison purposes, error covariance calculations were also performed using wideband ΔVLBI (ΔDOR) and narrowband ΔVLBI (ΔDOD) data which yielded angular precisions on the order of 0.07 to 0.4 μrad, and angular rate precisions on the order of 0.5 to 1.0×10^{-12} rad/sec.

[11] W. M. Folkner, Tracking Systems and Applications Section, personal communication, Jet Propulsion Laboratory, Pasadena, California, January 22, 1992.

[12] J. S. Border, "Analysis of ΔDOR and ΔDOD Measurement Errors for Mars Observer Using the DSN Narrow Channel Bandwidth VLBI System," Interoffice Memorandum 335.1-90-026 (internal document), Jet Propulsion Laboratory, Pasadena, California, May 15, 1990.

Acknowledgments

The authors thank Carl Christensen and John McNamee for their useful comments and suggestions in review of this article.

References

[1] S. W. Thurman, "Deep-Space Navigation With Differenced Data Types, Part I: Differenced Range Information Content," *TDA Progress Report 42-103*, July–September 1990, Jet Propulsion Laboratory, Pasadena, California, pp. 47–60, November 15, 1990.

[2] S. W. Thurman, "Deep-Space Navigation With Differenced Data Types, Part II: Differenced Doppler Information Content," *TDA Progress Report 42-103*, July–September 1990, Jet Propulsion Laboratory, Pasadena, California, pp. 61–69, November 15, 1990.

[3] S. C. Wu, "Atmospheric Media Effects on ARIES Baseline Determination," *TDA Progress Report 42-61*, November–December 1980, Jet Propulsion Laboratory, Pasadena, California, pp. 1–6, February 15, 1981.

[4] J. A. Klobuchar, *A First-Order, Worldwide, Ionosphere Time Delay Algorithm*, Document ARCRL-TR-75-0502, Air Force Cambridge Research Laboratories, Hanscom Air Force Base, Massachusetts, September 25, 1975.

[5] S. R. McReynolds, "The Sensitivity Matrix Method for Orbit Determination Error Analysis, With Applications to a Mars Orbiter," *JPL Space Programs Summary 37-56*, vol. 3, January–February 1969, pp. 85–87, March 31, 1969.

[6] G. J. Bierman, *Factorization Methods for Discrete Sequential Estimation*, San Diego, California: Academic Press, 1977.

[7] S. W. Thurman, "DSN Baseline Coordinate and Station Location Errors Induced by Earth Orientation Errors," *TDA Progress Report 42-103*, July–September 1990, Jet Propulsion Laboratory, Pasadena, California, pp. 40–46, November 15, 1990.

[8] J. S. Ulvestad and S. W. Thurman, "Orbit-Determination Performance of Doppler Data for Interplanetary Cruise Trajectories, Part I: Error Analysis Methodology," *TDA Progress Report 42-108*, October–December 1991, Jet Propulsion Laboratory, Pasadena, California, pp. 31–48, February 15, 1992.

[9] J. S. Ulvestad, "Orbit-Determination Performance of Doppler Data for Interplanetary Cruise Trajectories Part II: 8.4-GHz Performance and Data-Weighting Strategies," *TDA Progress Report 42-108*, October–December 1991, Jet Propulsion Laboratory, Pasadena, California, pp. 49–65, February 15, 1992.

Table 1. DSN station and baseline cylindrical coordinates.

Station	Location	r_s, km	z_h, km	λ, deg
DSS 14	Goldstone	5203.997	3677.052	243.1105
DSS 43	Canberra	5205.251	−3674.749	148.9813
DSS 63	Madrid	4862.451	4115.109	355.7520
Baseline	**Length, km**	r_B, km	z_B, km	λ_B, deg
DSS 43–14	10,588.966	7620.841	7351.801	286.0523
DSS 63–14	8,390.430	8378.986	−438.057	210.7265

Table 2. Differenced Doppler plus range angular precision using DSN Canberra–Goldstone baseline (computed-only results, 1σ).

Estimated parameter	Number of passes				
	1	2	3	4	5
			$\delta = -20$ deg		
δ_0, nrad	566.01	387.40	311.33	267.26	237.83
α_0, nrad	307.18	187.04	139.82	114.64	99.09
$\dot{\delta}_0$, prad/sec	21.23	13.40	10.36	8.75	7.76
$\dot{\alpha}_0$, prad/sec	10.13	6.11	4.50	3.62	3.06
			$\delta = -10$ deg		
δ_0, nrad	440.24	308.26	250.51	216.38	193.23
α_0, nrad	112.64	66.59	48.51	38.91	33.02
$\dot{\delta}_0$, prad/sec	12.08	7.55	5.85	4.98	4.47
$\dot{\alpha}_0$, prad/sec	10.23	5.96	4.24	3.31	2.73
			$\delta = 0$ deg		
δ_0, nrad	411.37	289.98	236.39	204.53	182.82
α_0, nrad	56.57	32.66	23.10	17.89	14.61
b_{T_1}, cm	300.00	212.15	173.22	150.02	134.18
b_{T_2}, cm	–	212.15	173.23	150.02	134.18
b_{T_3}, cm	–	–	173.23	150.02	134.18
b_{T_4}, cm	–	–	–	150.04	134.19
b_{T_5}, cm	–	–	–	–	134.21
$\dot{\delta}_0$, prad/sec	9.89	6.12	4.74	4.05	3.66
$\dot{\alpha}_0$, prad/sec	10.24	5.91	4.18	3.24	2.64
f_o, mm/sec	0.02	0.02	0.02	0.02	0.02
			$\delta = 10$ deg		
δ_0, nrad	438.62	307.27	249.77	215.77	192.70
α_0, nrad	110.26	65.28	47.63	38.27	32.53
$\dot{\delta}_0$, prad/sec	12.07	7.55	5.85	4.98	4.47
$\dot{\alpha}_0$, prad/sec	10.23	5.96	4.25	3.31	2.73
			$\delta = 20$ deg		
δ_0, nrad	561.34	384.56	309.20	265.52	236.33
α_0, nrad	304.68	185.80	139.10	114.18	98.81
b_{T_1}, cm	299.97	212.12	173.19	149.98	134.14
b_{T_2}, cm	–	212.12	173.19	149.98	134.14
b_{T_3}, cm	–	–	173.20	149.99	134.15
b_{T_4}, cm	–	–	–	150.01	134.15
b_{T_5}, cm	–	–	–	–	134.18
$\dot{\delta}_0$, prad/sec	21.19	13.38	10.35	8.74	7.76
$\dot{\alpha}_0$, prad/sec	10.14	6.11	4.50	3.62	3.06
f_o, mm/sec	0.02	0.02	0.02	0.02	0.02

Table 3. Differenced Doppler plus range angular precision using DSN Madrid–Goldstone baseline (computed-only results, 1σ).

Estimated parameter	Number of passes				
	1	2	3	4	5
	$\delta = 10$ deg				
δ_0, nrad	1207.32	762.43	594.71	509.12	458.51
α_0, nrad	393.96	277.10	225.54	194.87	173.97
$\dot{\delta}_0$, prad/sec	84.50	59.22	48.11	41.53	37.04
$\dot{\alpha}_0$, prad/sec	14.32	8.38	6.03	4.76	3.98
	$\delta = 20$ deg				
δ_0, nrad	324.05	224.20	190.60	175.09	166.63
α_0, nrad	379.64	266.01	215.31	184.88	163.99
b_{T_1}, cm	294.50	206.39	167.03	143.40	127.18
b_{T_2}, cm	–	206.39	167.04	143.41	127.18
b_{T_3}, cm	–	–	167.04	143.41	127.18
b_{T_4}, cm	–	–	–	143.43	127.19
b_{T_5}, cm	–	–	–	–	127.21
$\dot{\delta}_0$, prad/sec	39.77	27.82	22.50	19.31	17.12
$\dot{\alpha}_0$, prad/sec	8.23	4.88	3.58	2.90	2.49
f_o, mm/sec	0.02	0.02	0.02	0.02	0.02

Table 4. Differenced Doppler plus range angular precision using DSN Canberra–Goldstone baseline (full-consider results, 1σ).

Estimated parameter	Number of passes				
	1	2	3	4	5
	$\delta = -20$ deg				
δ_0, nrad	675.03	534.78	483.21	456.86	441.18
α_0, nrad	498.46	435.05	417.21	409.79	406.10
$\dot{\delta}_0$, prad/sec	33.37	29.02	27.74	27.18	26.88
$\dot{\alpha}_0$, prad/sec	15.42	13.14	12.48	12.20	12.05
	$\delta = -10$ deg				
δ_0, nrad	474.99	356.27	307.83	280.95	263.76
α_0, nrad	201.46	179.86	174.03	171.68	170.53
$\dot{\delta}_0$, prad/sec	19.49	17.06	16.38	16.09	15.94
$\dot{\alpha}_0$, prad/sec	15.57	13.16	12.48	12.19	12.05
	$\delta = 0$ deg				
δ_0, nrad	431.60	318.02	270.05	242.64	224.64
α_0, nrad	128.48	119.89	117.64	116.73	116.27
b_{T_1}, cm	300.00	212.15	173.22	150.02	134.18
b_{T_2}, cm	–	212.15	173.23	150.02	134.18
b_{T_3}, cm	–	–	173.23	150.02	134.18
b_{T_4}, cm	–	–	–	150.04	134.19
b_{T_5}, cm	–	–	–	–	134.21
$\dot{\delta}_0$, prad/sec	16.45	14.50	13.97	13.76	13.65
$\dot{\alpha}_0$, prad/sec	15.53	13.09	12.41	12.12	11.98
f_o, mm/sec	0.02	0.02	0.02	0.02	0.02
	$\delta = 10$ deg				
δ_0, nrad	472.99	354.75	306.47	279.66	262.50
α_0, nrad	119.78	178.97	173.38	171.12	170.02
$\dot{\delta}_0$, prad/sec	19.48	17.05	16.37	16.08	15.93
$\dot{\alpha}_0$, prad/sec	15.53	13.11	12.43	12.14	12.00
	$\delta = 20$ deg				
δ_0, nrad	668.69	529.70	478.56	452.43	436.90
α_0, nrad	496.29	433.83	416.28	409.00	405.41
b_{T_1}, cm	299.98	212.16	173.27	150.13	134.39
b_{T_2}, cm	–	212.16	173.28	150.14	134.39
b_{T_3}, cm	–	–	173.29	150.14	134.39
b_{T_4}, cm	–	–	–	150.16	134.40
b_{T_5}, cm	–	–	–	–	134.42
$\dot{\delta}_0$, prad/sec	33.32	28.99	27.72	27.17	26.87
$\dot{\alpha}_0$, prad/sec	15.34	13.05	12.38	12.10	11.95
f_o, mm/sec	0.02	0.02	0.02	0.02	0.02

Table 5. Differenced Doppler plus range angular precision using Madrid–Goldstone baseline (full-consider results 1σ).

Estimated parameter	Number of passes				
	1	2	3	4	5
	$\delta = 10$ deg				
δ_0, nrad	2264.36	2057.61	1997.18	1968.97	1952.06
α_0, nrad	410.51	300.00	253.87	228.87	214.37
$\dot{\delta}_0$, prad/sec	92.11	68.40	57.76	51.16	46.45
$\dot{\alpha}_0$, prad/sec	26.52	23.83	23.09	22.77	22.61
	$\delta = 20$ deg				
δ_0, nrad	624.82	578.70	565.86	560.16	556.92
α_0, nrad	387.24	285.02	251.82	244.03	249.26
b_{T_1}, cm	299.48	221.39	197.27	192.83	198.24
b_{T_2}, cm	–	221.39	197.27	192.83	198.24
b_{T_3}, cm	–	–	197.27	192.83	198.24
b_{T_4}, cm	–	–	–	192.84	198.24
b_{T_5}, cm	–	–	–	–	198.24
$\dot{\delta}_0$, prad/sec	40.22	28.26	23.29	21.01	20.32
$\dot{\alpha}_0$, prad/sec	15.65	14.17	13.77	13.60	13.52
f_o, mm/sec	0.02	0.02	0.02	0.02	0.02

Table 6. ΔVLBI angular precision (1σ) using DSN Goldstone–Canberra baseline (results for five consecutive passes).

Estimated parameter	Number of passes				
	−20	−10	0	10	20
	$\delta = 10$ deg				
δ_0, nrad	71.0	115.0	235.0	384.0	152.0
α_0, nrad	92.6	127.0	236.0	369.0	150.0
$\dot{\delta}_0$, prad/sec	0.55	1.35	0.98	1.22	0.51
$\dot{\alpha}_0$, prad/sec	0.56	1.30	1.00	1.18	0.53

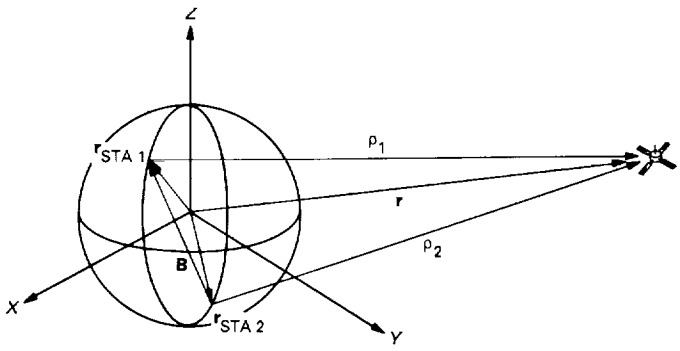

Fig. 1. Differenced range measurement geometry.

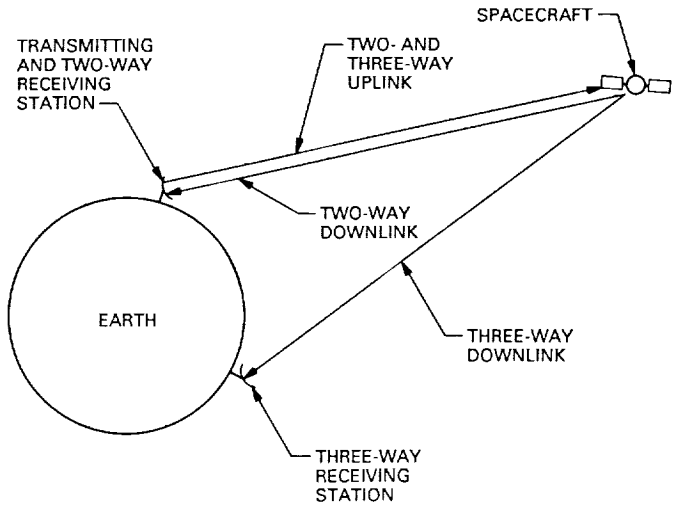

Fig. 3. Differenced Doppler and range data acquisition scheme.

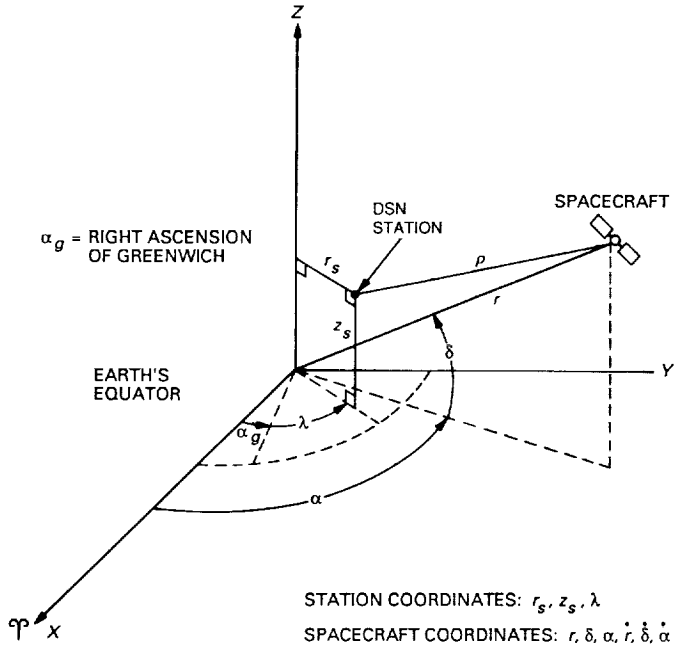

Fig. 2. Spacecraft and DSN station coordinates.

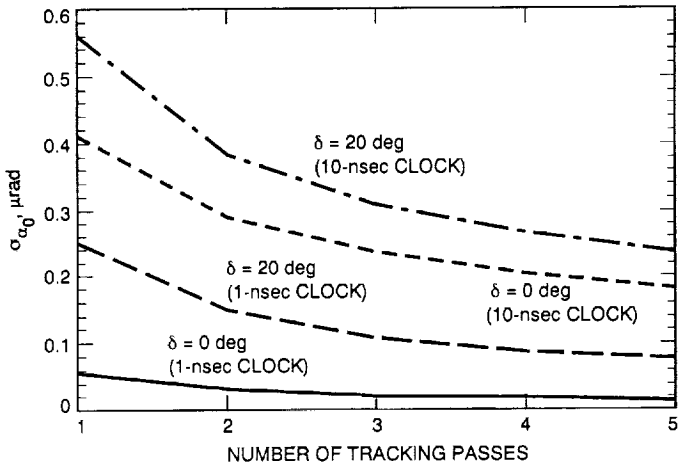

Fig. 4. Comparison of Canberra–Goldstone baseline declination precision for varying clock bias values.

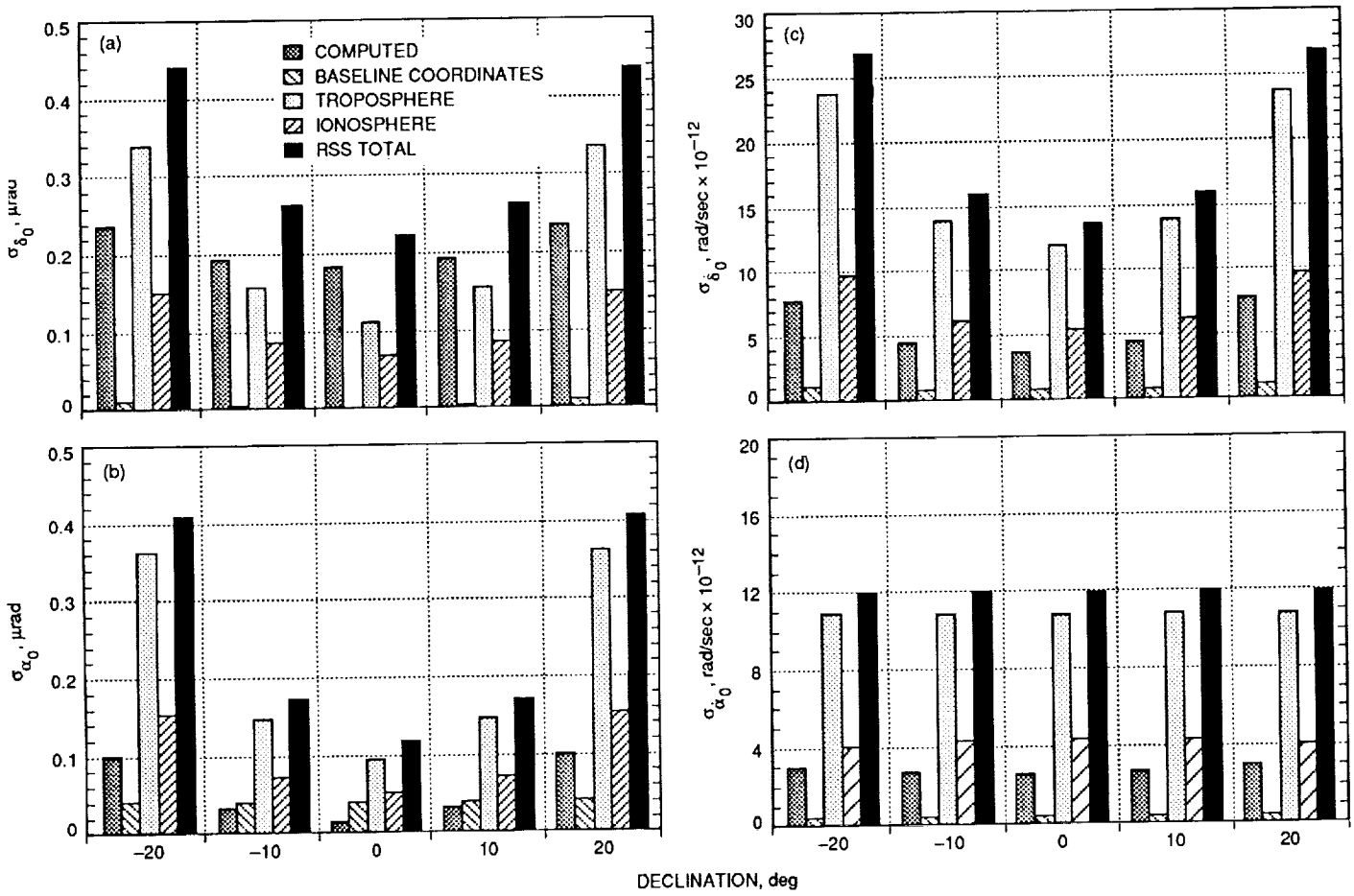

Fig. 5. Angular precision in terms of individual error sources for DSN Canberra–Goldstone baseline: (a) epoch declination uncertainty; (b) epoch right ascension uncertainty; (c) epoch declination rate; and (d) epoch right ascension rate.

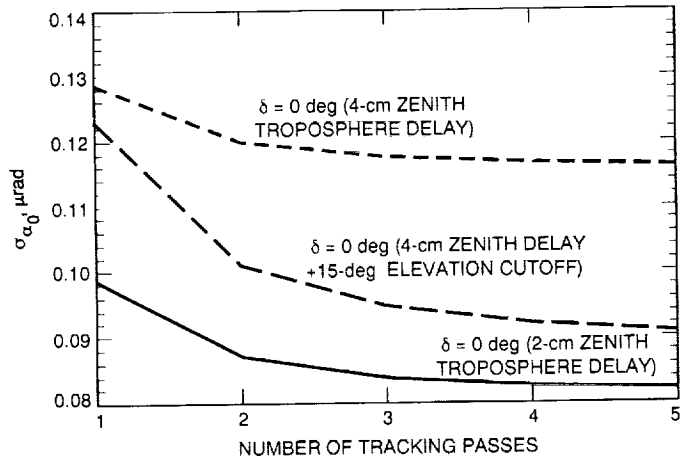

Fig. 6. Performance comparison for various troposphere path-delay reduction schemes using DSN Canberra–Goldstone baseline.